05

Synthesis and properties of the $LiMgFe_2(VO_4)_3$ with frustrated magnetic interactions

© T.V. Drokina, M.S. Molokeev, O.A. Bayukov, D.A. Velikanov, A.M. Vorotynov

Kirensky Institute of Physics, Siberian Branch of the Russian Academy of Sciences, Krasnoyarsk, Russia

E-mail: tvd@iph.krasn.ru

Received June 23, 2025
Revised July 16, 2025
Accepted July 17, 2025

We have investigated structural, static magnetic and resonance properties of the new $LiMgFe_2(VO_4)_3$ magnetic, which is produced from initial oxides Li_2CO_3, Fe_2O_3, MgO and V_2O_5 by solid-phase synthesis. Specific features of the trigonal crystalline $LiMgFe_2(VO_4)_3$ structure with mixed Mg^{2+}/Fe^{3+} cations in the same site with a symmetry described by a noncentrosymmetric space group $P1$ allow existence of competing magnetic exchange interactions with a high level of magnetic frustrations. We have found a dependence of static magnetic susceptibility on sample cooling conditions, which is typical for a spin-glass magnetic state.

Keywords: new organic compounds, multi-component vanadates, crystalline structure, magnetic properties.

DOI: 10.61011/PSS.2025.08.62260.167-25

1. Introduction

Vanadates, including those with a general formula $AMeFe_2(VO_4)_3$, where A are monovalent alkaline earth elements ($A = \mathrm{Li, Na}$), Me are bivalent elements ($Me = \mathrm{Ni, Cu, Zn, Mn}$), are oxide compounds with centrosymmetric and noncentrosymmetric crystalline structures [1–4], which cause origination of competing exchange interactions in the magnetic subsystem, thereby attracting attention to them in terms of both fundamental physics and possible applications as well. Availability of introduction of various cations of the bivalent metals into a crystal lattice of the multi-components vanadates also makes them an object for searching new magnetic materials. This was the motivation for producing the $LiMgFe_2(VO_4)_3$ compound. The present article provides results of investigation of the structural, resonance and magnetic properties of the new $LiMgFe_2(VO_4)_3$ compound.

2. Sample synthesis and experimental technique

The $LiMgFe_2(VO_4)_3$ samples were produced by a solid-phase reaction from a mixture of the powder-like high-purity oxides Li_2CO_3, Fe_2O_3, MgO, V_2O_5 with annealings at the temperature of 640 °C for 24 h in air. The chemical and phase composition of the synthesized samples was controlled via X-ray diffraction analysis.

An X-ray powder diffraction pattern of $LiMgFe_2(VO_4)_3$ was recorded at the room temperature using the Haoyuan DX-2700BH diffractometer (equipment of the Krasnoyarsk Regional Center of Research Equipment of the Federal Research Center - „Krasnoyarsk Science Center of the Siberian Branch of the Russian Academy of Sciences“) with Cu$K\alpha$ radiation and a linear detector. An increment of 2θ was 0.01°, the count time was 0.2 s per increment.

The electron magnetic resonance spectra were taken on a Bruker Elexsys E580 spectrometer in the X-range ($\nu = 9$ GHz) and the temperature range 110−300 K. The following parameters were used for spectrum recording: the microwave power — 0.63 mW, the modulation amplitude — 0.7 G, the modulation frequency — 10 kHz, the magnetic field sweep width — 5 kG, the sweep time — 40 s.

The nuclear gamma-resonance spectra were recorded using the MS-1104Em spectrometer of the Kirensky Institute of Physics of the Siberian Branch of RAS at the room temperature with a source of Co^{57}(Rh) on powder absorbers of the mass 5−1 mg per 1 cm^2 with respect to the natural iron content. The chemical shift values are given relative to α-Fe.

The static magnetic properties of $LiMgFe_2(VO_4)_3$ were studied using the SQUID magnetometer originally designed by the Kirensky Institute of Physics of Federal Research Center KSC of Siberian Branch of RAS [5]. The static magnetic characteristics were measured within the temperature range 4−300 K in two modes: cooling of the sample without a magnetic field (ZFC) and in a magnetic field (FC).

3. Experimental results and discussion

3.1. Structural investigation data

The $LiMgFe_2(VO_4)_3$ structure was investigated using X-ray diffraction and Mössbauer spectroscopy.

Figure 1 shows a powder X-ray pattern of $LiMgFe_2(VO_4)_3$, which is obtained at the room temperature. Almost all reflections were indexed by a triclinic

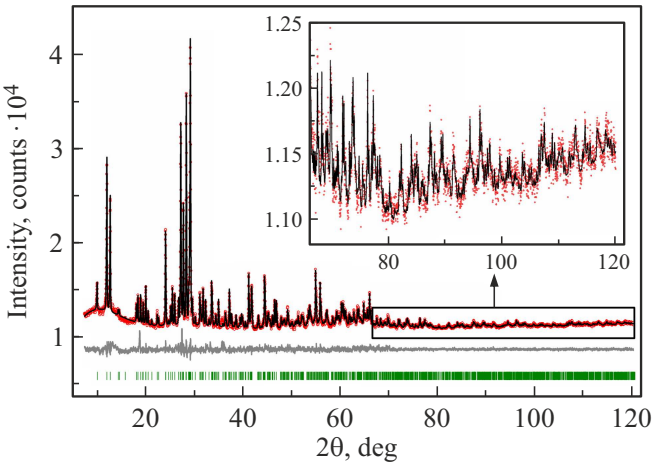

Figure 1. X-ray pattern of the polycrystalline $LiMgFe_2(VO_4)_3$ compound at the temperature $T = 300$ K. The lower curve marks a differential X-ray diffraction pattern.

Table 1. (a, b, c, α, β, γ are the lattice cell parameters; V is the cell volume; 2θ is the measurement interval; unreliability factors: R_{wp} — the weight profile factor, R_p — the profile factor, R_B — the integral factor; χ^2 — the fitting quality) and the results of refinement of the crystalline $LiMgFe_2(VO_4)_3$ structure at the temperature $T = 300$ K

Parameter	Value
Space group	$P1$
a, Å	6.7226(1)
b, Å	8.0825(2)
c, Å	9.8059(2)
α, deg	106.040(1)
β, deg	104.445(1)
γ, deg	101.779(1)
V, Å^3	474.05(2)
Z	2
2θ-interval, deg	5–120
Number of reflections	1419
Number of the refined parameters	166
R_{wp}, %	1.08
R_p, %	0.92
R_B, %	0.37
χ^2	1.69

cell with parameters close to those of $NaFe_3(VO_4)_3$ [6]; therefore this structure was used an initial one. Two independent Na ions were substituted with Li ions, while all six sites of Fe ions were populated with Fe/Mg ions with refined site occupancies with taking into account that a sum of the occupancies in each site is equal to 1. The coordinates of Li1 were not refined, which is needed to fix the origin in a polar group $P1$. Rietveld refinement was implemented using TOPAS 4.2 software [7]. The results of the refinement are shown in Table 1 and Figure 1.

The atom coordinates in the crystalline structure, the site occupancy and the thermal parameters are given in Table 2.

Main bond lengths in the crystalline $LiMgFe_2(VO_4)_3$ structure at the temperature of $T = 300$ K are shown in Table 3.

The compound structure is shown in Figure 2. The chemical formula of the compound, which is based on the results of refinement of the $Li_2Mg_{0.9(1)}Fe_{2.1(1)}(VO_4)_3$ structure is close to the one assumed from the synthesis.

Table 2. Atom coordinates, isotropic thermal parameters B_{iso} and site occupancy in the crystalline $LiMgFe_2(VO_4)_3$ structure when $T = 300$ K

Atom	x/a	y/b	z/c	B_{iso}, Å^2	Occ.
Li1	0.9894	0.0242	0.5534	0.5(18)	1
Li2	0.25(3)	0.90(2)	0.393(17)	0.5(18)	1
Fe1	0.13(2)	0.550(17)	0.398(14)	0.5(7)	0.870(96)
Mg1	0.13(2)	0.550(17)	0.398(14)	0.5(7)	0.130(96)
Fe2	0.88(2)	0.445(17)	0.609(14)	0.5(7)	0.646(88)
Mg2	0.88(2)	0.445(17)	0.609(14)	0.5(7)	0.354(88)
Fe3	0.46(2)	0.298(16)	0.990(13)	0.5(6)	0.93(10)
Mg3	0.46(2)	0.298(16)	0.990(13)	0.5(6)	0.07(10)
Fe4	0.55(2)	0.712(16)	0.013(13)	0.5(8)	0.415(99)
Mg4	0.55(2)	0.712(16)	0.013(13)	0.5(8)	0.585(99)
Fe5	0.79(2)	0.778(16)	0.795(13)	0.5(6)	0.825(76)
Mg5	0.79(2)	0.778(16)	0.795(13)	0.5(6)	0.175(76)
Fe6	0.23(2)	0.220(17)	0.197(14)	0.5(7)	0.488(77)
Mg6	0.23(2)	0.220(17)	0.197(14)	0.5(7)	0.512(77)
V1	0.38(2)	0.388(17)	0.659(14)	0.50(17)	1
V2	0.60(2)	0.584(16)	0.330(13)	0.50(17)	1
V3	0.28(2)	0.829(16)	0.730(14)	0.50(17)	1
V4	0.73(2)	0.148(17)	0.263(14)	0.50(17)	1
V5	0.09(2)	0.782(17)	0.127(13)	0.50(17)	1
V6	0.92(2)	0.232(17)	0.887(13)	0.50(17)	1
O1	0.42(2)	0.423(18)	0.850(15)	0.5(3)	1
O2	0.54(2)	0.563(19)	0.126(15)	0.5(3)	1
O3	0.33(3)	0.491(19)	0.356(15)	0.5(3)	1
O4	0.63(3)	0.539(19)	0.662(15)	0.5(3)	1
O5	0.27(3)	0.815(18)	0.568(16)	0.5(3)	1
O6	0.73(3)	0.207(18)	0.455(16)	0.5(3)	1
O7	0.47(3)	0.213(19)	0.164(15)	0.5(3)	1
O8	0.49(3)	0.758(19)	0.824(15)	0.5(3)	1
O9	0.15(2)	0.243(17)	0.012(15)	0.5(3)	1
O10	0.87(2)	0.691(17)	0.997(15)	0.5(3)	1
O11	0.17(3)	0.443(18)	0.554(16)	0.5(3)	1
O12	0.85(3)	0.525(19)	0.414(15)	0.5(3)	1
O13	0.04(2)	0.758(18)	0.748(14)	0.5(3)	1
O14	0.99(3)	0.274(17)	0.251(15)	0.5(3)	1
O15	0.32(3)	0.05(2)	0.827(15)	0.5(3)	1
O16	0.67(3)	0.938(18)	0.200(15)	0.5(3)	1
O17	0.36(3)	0.19(2)	0.566(17)	0.5(3)	1
O18	0.64(3)	0.791(19)	0.430(17)	0.5(3)	1
O19	0.15(2)	0.000(17)	0.231(14)	0.5(3)	1
O20	0.78(2)	1.004(18)	0.734(15)	0.5(3)	1
O21	0.26(3)	0.747(17)	0.027(14)	0.5(3)	1
O22	0.77(2)	0.315(17)	0.985(15)	0.5(3)	1
O23	0.11(2)	0.653(18)	0.254(15)	0.5(3)	1
O24	0.96(2)	0.309(17)	0.731(15)	0.5(3)	1

It follows from analysis of the results of the X-ray diffraction research that the $LiMgFe_2(VO_4)_3$ compound is crystallized in the triclinic structure. The symmetry of the crystal structure is described by the noncentrosymmetric space group $P1$. The lattice cell contains two formula units ($Z = 2$). Iron cations in the crystal lattice are distributed along six nonequivalent sites and mixed with magnesium cations. The mixed sites of Fe^{3+}/Mg^{2+} have a different environment by oxygen anions that form octahedrons (6 oxygen atoms) and trigonal bipyramids (5 oxygen atoms). The four sites have the octahedral oxygen environment and the two sites have the environment in the form of the trigonal bipyramid. The compounds $(Fe_i^{3+}/Mg_i^{2+})O_j$ are interconnected by common vertices and form infinite chains $(\ldots-(Fe^{3+}1/Mg^{2+}1)-(Fe^{3+}2/Mg^{2+}2)-(Fe^{3+}5/Mg^{2+}5)-(Fe^{3+}4/Mg^{2+}4)-(Fe^{3+}3/Mg^{2+}3)-(Fe^{3+}6/Mg^{2+}6)-\ldots)$ stretching along the direction **a**−**c**. The chains are connected to each other by tetrahedral anionic complexes $(VO_4)^{3-}$, forming a two-dimensional layer in a plane based on two vectors **a**−**c** and **b**. The layers that are bound by bundles VO_4 form a three-dimensional structure. Channels of the structure are filled with cations Na^+, which occupy two nonequivalent crystallographic sites.

Table 3. Main bond lengths in the crystalline $LiMgFe_2(VO_4)_3$ structure when $T = 300$ K

Bond	Length, Å	Bond	Length, Å
Li1−O6	2.66(11)	Mg4−O1^{vi}	2.28(15)
Li1−O17^{i}	2.53(10)	Mg4−O2	1.85(15)
Li1−O18^{ii}	2.47(11)	Mg4−O8^{vi}	1.95(17)
Li1−O20^{ii}	2.53(11)	Mg4−O10^{vi}	2.21(14)
Li1−O24	2.56(11)	Mg4−O16	2.04(16)
Li2−V5	2.38(19)	Mg4−O21	2.11(14)
Li2−O5	1.98(19)	Fe5−O4	1.91(15)
Li2−O17^{iii}	2.32(18)	Fe5−O8	2.14(14)
Li2−O19^{iii}	2.03(17)	Fe5−O10	2.26(16)
Li2−O23	1.92(17)	Fe5−O13^{i}	1.88(14)
Fe1−O3	1.66(14)	Fe5−O20	2.08(13)
Fe1−O5	2.16(16)	Mg5−O4	1.91(15)
Fe1−O11	1.95(16)	Mg5−O8	2.14(14)
Fe1−O12^{iv}	1.90(14)	Mg5−O10	2.26(16)
Fe1−O14^{iv}	2.15(15)	Mg5−O13^{i}	1.88(14)
Fe1−O23	1.82(16)	Mg5−O20	2.08(13)
Mg1−O3	1.66(14)	Fe6−O3	2.16(16)
Mg1−O5	2.16(16)	Fe6−O7	1.76(14)
Mg1−O11	1.95(16)	Fe6−O9	1.83(17)
Mg1−O12^{iv}	1.90(14)	Fe6−O14^{iv}	1.92(14)
Mg1−O14^{iv}	2.15(15)	Fe6−O19	1.89(13)
Mg1−O23	1.82(16)	Mg6−O3	2.16(16)
Fe2−O4	2.10(15)	Mg6−O7	1.76(14)
Fe2−O6	1.96(16)	Mg6−O9	1.83(17)
Fe2−O11^{i}	2.12(15)	Mg6−O14^{iv}	1.92(14)
Fe2−O12	2.16(17)	Mg6−O19	1.89(13)
Fe2−O13^{i}	2.38(14)	V1−O1	1.76(18)
Fe2−O24	1.88(15)	V1−O4	1.84(14)
Mg2−O4	2.10(15)	V1−O11	1.77(16)
Mg2−O6	1.96(16)	V1−O17	1.59(15)
Mg2−O11i	2.12(15)	V2−O2	1.89(17)
Mg2−O12	2.16(17)	V2−O3	1.91(14)
Mg2−O13^{i}	2.38(14)	V2−O12	1.87(14)
Mg2−O24	1.88(15)	V2−O18	1.62(15)
Fe3−O1	1.92(15)	V3−O5	1.55(18)
Fe3−O2^{v}	2.06(15)	V3−O8	1.77(15)
Fe3−O7^{v}	200(16)	V3−O13	1.62(13)
Fe3−O9^{v}	2.15(14)	V3−O15^{iii}	1.67(15)
Fe3−O15	2.06(16)	V4−O6	1.80(19)
Fe3−O22	2.05(14)	V4−O7	1.99(15)
Mg3−O1	1.92(15)	V4−O14	1.88(14)
Mg3−O2^{v}	2.06(15)	V4−O16^{ii}	1.57(14)
Mg3−O7^{v}	200(16)	V5−O10^{vii}	1.58(16)
Mg3−O9^{v}	2.15(14)	V5−O19^{iii}	1.68(14)
Mg3−O15	2.06(16)	V5−O21	1.66(15)
Mg3−O22	2.05(14)	V5−O23	1.83(15)
Fe4−O1^{vi}	2.28(15)	V6−O9^{viii}	1.68(15)
Fe4−O2	1.85(15)	V6−O20^{ii}	1.89(16)
Fe4−O8^{vi}	1.95(17)	V6−O22	1.67(15)
Fe4−O10^{vi}	2.21(14)	V6−O24	1.86(16)
Fe4−O16	2.04(16)	O1−O2^{v}	2.47(19)
Fe4−O21	2.11(14)	O1−O8	2.75(14)

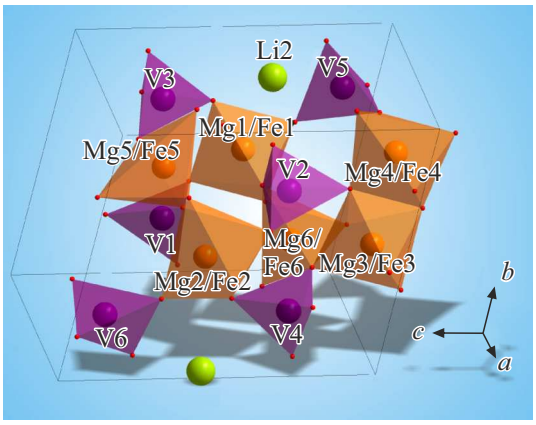

Figure 2. Crystal structure of $LiMgFe_2(VO_4)_3$.

It can be expected that structural disorder in distribution of the iron cations in $LiMgFe_2(VO_4)_3$ affects magnetic properties of the compound.

The charge composition of the compound is as follows: $Li^+Mg^{2+}Fe_2^{3+}(V^{5+}O_4^{2-})_3$. A state of local violation of charge neutrality is observed due to mixing of the Fe^{3+} cations with the Mg^{2+} magnesium cations in the lattice cell at the same site.

The state of the iron cations in the $LiMgFe_2(VO_4)_3$ vanadate is studied using a method based on the Mössbauer effect. The spectrum of nuclear gamma-resonance at the room temperature in $LiMgFe_2(VO_4)_3$ is shown in Figure 3. The Mössbauer spectrum is a sum of two doublets. The spectrum parameters are given in Table 4.

It follows from the Mössbauer spectroscopy data that the iron cations in $LiMgFe_2V_3O_{12}$ are in a high-spin state of Fe^{3+} ($S = 5/2$, $3d^5$) and distributed along two sites that are nonequivalent in terms of the environment by the oxygen atoms. The sites of the iron cations have

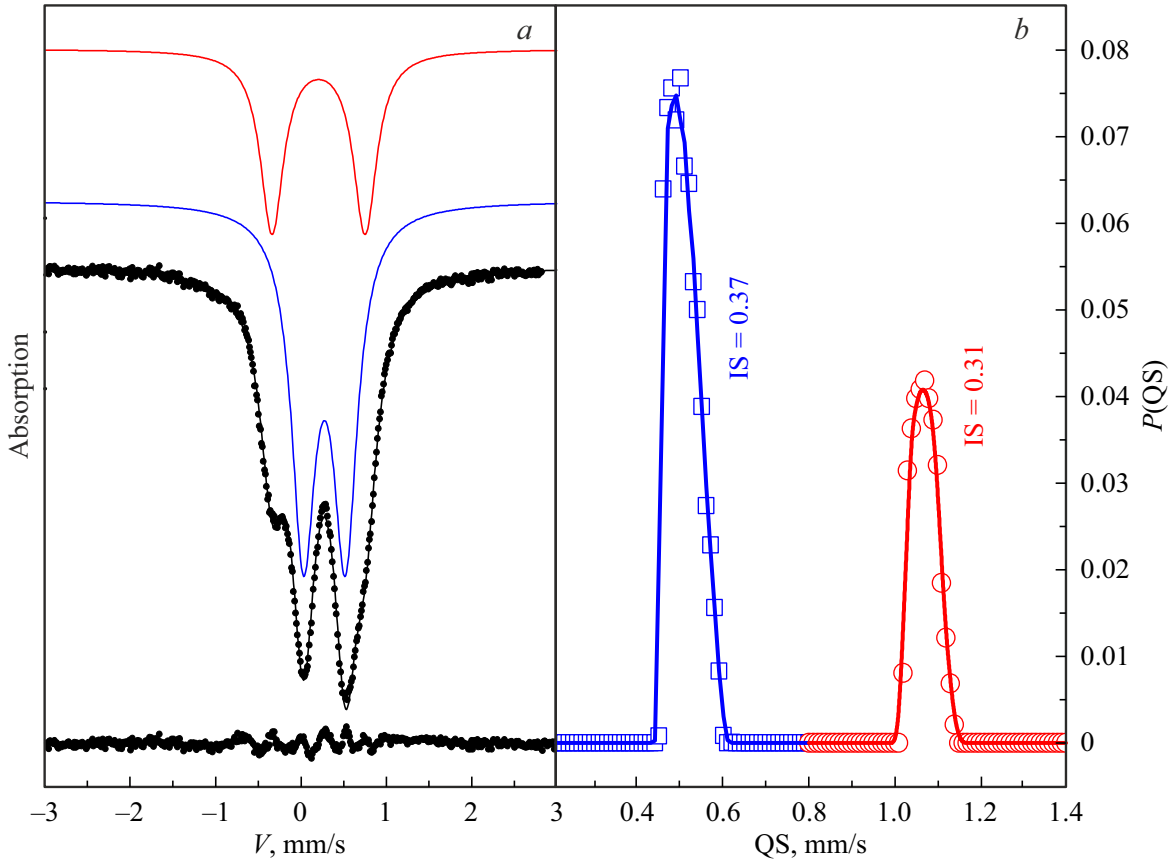

Figure 3. *a* — the Mössbauer spectrum of $LiMgFe_2V_3O_{12}$ as measured at the room temperature. The color lines mark spectrum components, whose parameters are given in Table 4. The difference between the experimental and calculated spectra is shown below. *b* — probability distribution of quadrupole splitting in the experimental spectrum, based on which a model spectrum is formed for fitting to the experimental one.

Table 4. Mössbauer parameters of ^{57}Fe in $LiMgFe_2V_3O_{12}$: IS — the isomeric chemical shift relative to α-Fe, QS — the quadrupole splitting, W — the absorption line width, A — the occupancy of nonequivalent iron sites

IS, mm/s ±0.01	QS, mm/s ±0.02	W, mm/s ±0.02	A, at.% ±0.05	Site
0.37	0.47	0.32	0.66	$Fe^{3+}(6)$
0.31	1.04	0.31	0.34	$Fe^{3+}(5)$

chemical shifts IS = 0.37 and 0.31 mm/s relative to α-Fe and quadrupole splittings QS = 0.47 and 1.04 mm/s, which belong to octahedral and bipyramidal oxygen environments, respectively. The occupancy of the iron sites with the octahedral oxygen environment in two times exceeds the occupancy of the sites with the bipyramidal environment.

3.2. Results of EPR investigation of $LiMgFe_2V_3O_{12}$

The spectra of electron paramagnetic resonance (EPR) in $LiMgFe_2V_3O_{12}$ are studied at the frequency of 9 GHz within the temperature interval 110–300 K in the external magnetic field H up to 7000 Oe. Figure 4, *a* shows the EPR spectrum at the room temperature. Figure 4, *b* shows a result of fitting of the experimental EPR spectrum by two Lorentz-shaped absorption curves *1* and *2*.

Figure 5 show the temperature dependences of the intensity I (*a*), the resonance field H_{res} (*b*) and the line width dH (*c*) for the fitting curves *1* and *2*.

It follows from the EPR data that the signal *2* is induced by the main $LiMgFe_2V_3O_{12}$ matrix. The intensity of this signal is by an order of magnitude higher than that of the signal *1*. The line *1* is probably associated with formation of a small amount of hematite-phase superparamagnetic particles upon implantation of the bivalent magnesium cations in the process of synthesis. This assumption is also supported by specific features of the temperature dependences of the resonance field: the value of the resonance field of the signal *1* decreases with decreasing temperature, whereas the resonance field of the signal *2* is virtually independent of the temperature.

When $T = 297.8$ K, values of the Lande g-actors for the curves *2* and *1* are $g(2) = 1.978$ and $g(1) = 2.692$, respectively.

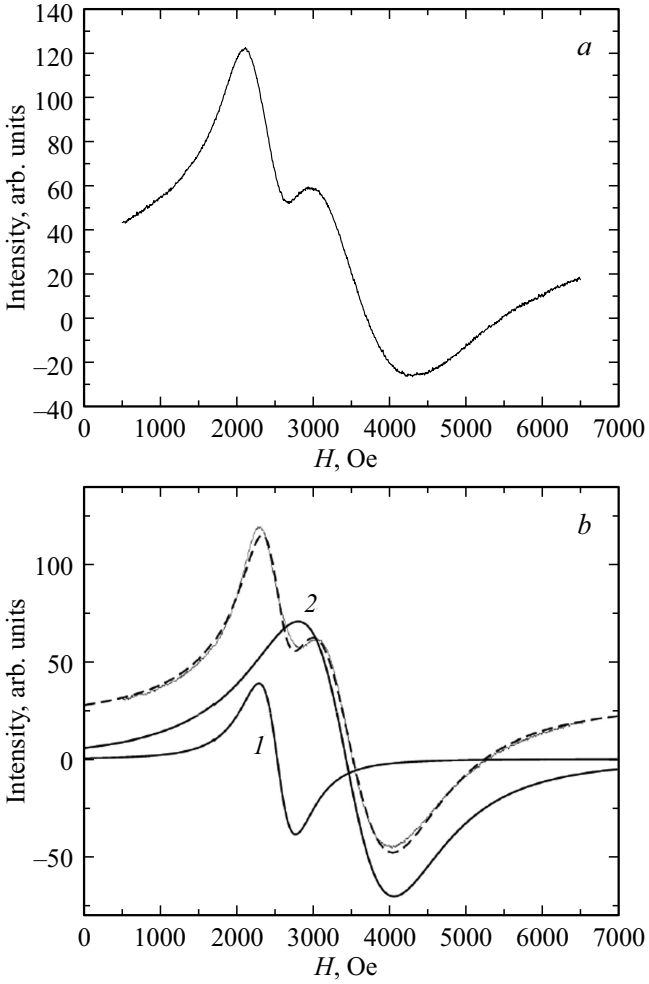

Figure 4. *a* — the EPR spectrum of $LiMgFe_2V_3O_{12}$ at the frequency of 9 GHz at the room temperature;n *b* — the result of fitting of the experimental EPR spectrum by the two Lorentz-shaped absorption curves *1* and *2*.

3.3. Results of static magnetic measurements of $LiMgFe_2V_3O_{12}$

The magnetic subsystem of $LiMgFe_2V_3O_{12}$ is formed by magnetic iron cations Fe^{3+} ($S = 5/2$). The metals magnesium Mg^{2+} and vanadium V^{5+} are nonmagnetic. Thus, the magnetic properties of the lithium-magnesium vanadate are determined by four high-spin iron cations which occupy six nonequivalent sites in the crystal lattice together with the magnesium cations.

Figure 6 shows the temperature dependences of magnetic susceptibility χ and inverse magnetic susceptibility χ^{-1}, which are measured in the magnetic field $H = 10$ Oe (the sample mass is $M = 0.060$ g).

It follows from the experiment that paramagnetic susceptibility of $LiMgFe_2V_3O_{12}$ within the temperature range 40–300 K follows the Curie-Weiss law with the asymptotic Néel temperature $\theta = -97$ K. The negative value of θ indicates a predominant role of antiferromagnetic exchange interactions between the Fe^{3+} cations in the magnetic subsystem of the sample.

In the temperature region with the linear temperature dependence of inverse magnetic susceptibility, the $LiMgFe_2V_3O_{12}$ compound is a paramagnetic with a molar value of the effective magnetic moment $\mu_{eff(ex)} = 8.57\,\mu_B$. The calculated value of the formula unit's effective magnetic moment is $\mu_{eff(calc.)} = 8.36\,\mu_B$.

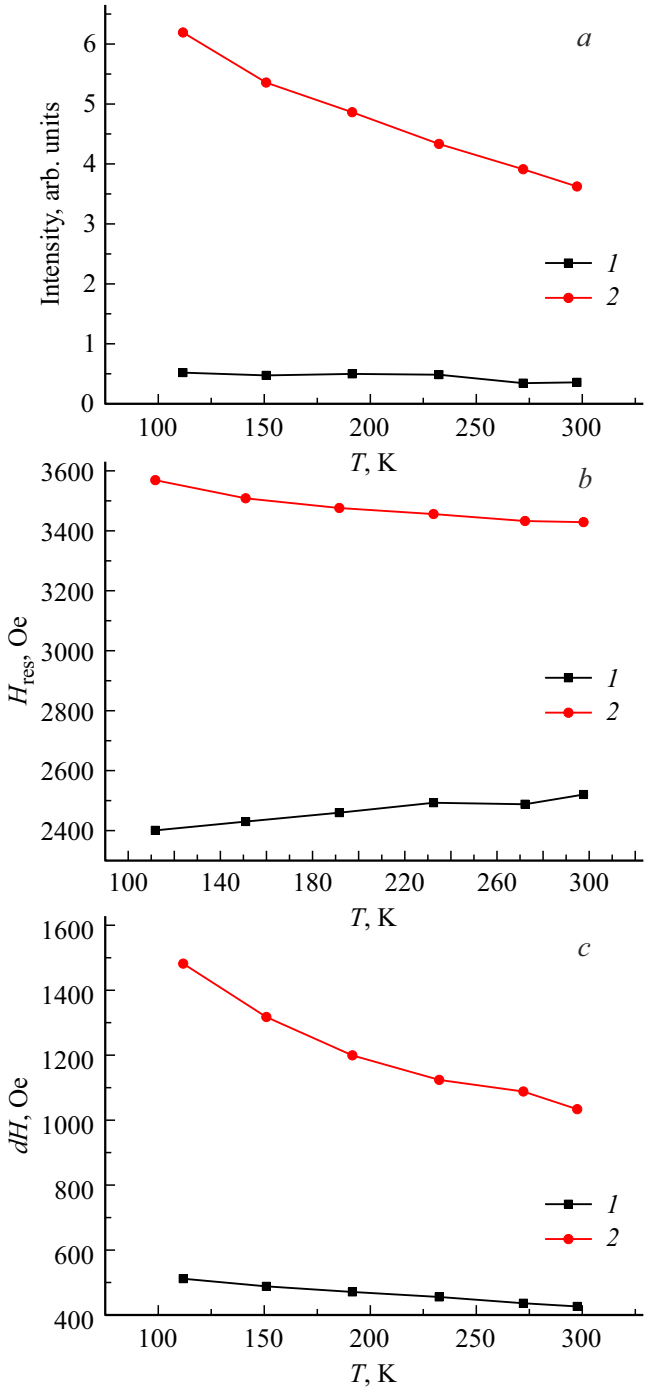

Figure 5. Temperature dependences of: *a* — the intensity, *b* — the resonance field H_{res}, *c* — the EPR signal width *dH* at the frequency of $\nu = 9$ GHz in $LiMgFe_2V_3O_{12}$.

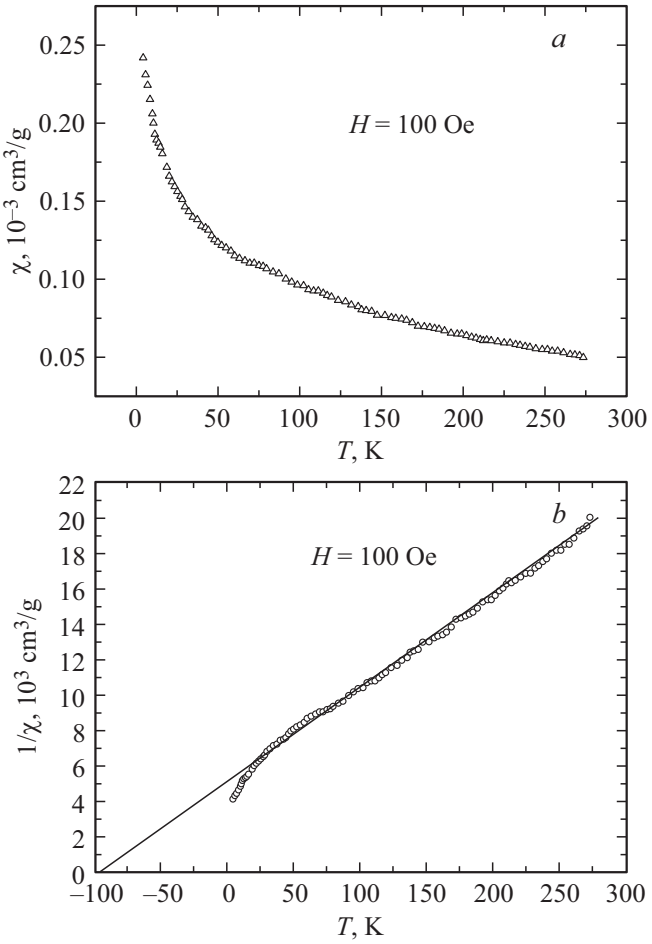

Figure 6. Temperature dependences of magnetic susceptibility χ and inverse magnetic susceptibility χ^{-1} in $LiMgFe_2V_3O_{12}$, which are measured in the magnetic field $H = 100$ Oe. The sample mass is $M = 0.060$ g.

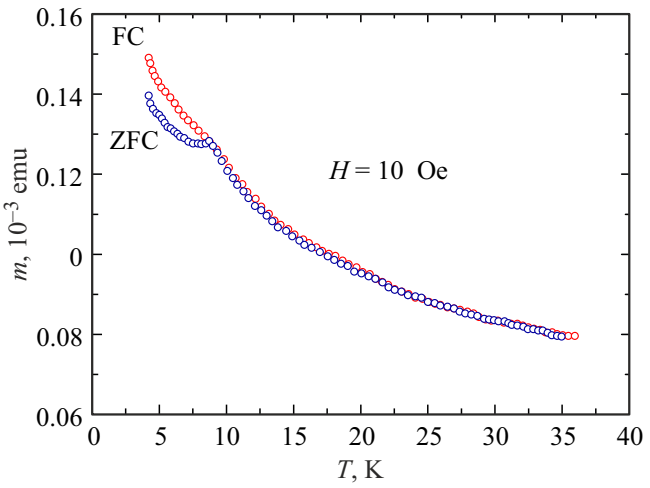

Figure 7. Temperature dependences of the magnetic moment m in $LiMgFe_2V_3O_{12}$ when cooling the sample in the external magnetic field $H = 10$ Oe (FC) and without the field (ZFC). The measurement is carried out in the magnetic field $H = 10$ Oe. The temperature of divergence of the curves ZFC and FC is $T_F = 8.8$ K.

As shown in Figure 7, a progress of the temperature dependence of the magnetic moment in $LiMgFe_2V_3O_{12}$ in a region of the low temperatures (below the temperature $T_F = 8.8$ K) depends on conditions of sample cooling in the external magnetic field $H = 10$ Oe (FC)and without the field (ZFC), which is one of the characteristics of the magnetic state of spin glass [8,9].

As a result of disordered distribution of the iron cations Fe^{3+} and the nonmagnetic magnesium cations Mg^{2+} along the six nonequivalent sites in the crystal lattice of $LiMgFe_2(VO_4)_3$, we should expect presence of significant magnetic frustrations. A level of magnetic frustrations f can be evaluated using the relationship $f \approx |\theta|/T_c$, where T_c is a critical temperature, below which a magnetic order is established [10,11]. For the $LiMgFe_2V_3O_{12}$ compound, the level of magnetic frustrations is $f \approx 11$.

4. Conclusion

The new $LiMgFe_2V_3O_{12}$ magnetic compound is produced from the initial oxides Li_2CO_3, Fe_2O_3, MgO and V_2O_5 by solid-phase synthesis. The structural, static magnetic properties are studied and the material is characterized by means the Mössbauer spectroscopy and the electron paramagnetic resonance.

The investigation results experimentally prove that $LiMgFe_2V_3O_{12}$ has significant magnetic frustrations that are induced by disordered distribution of the magnetic iron cations Fe^{3+} mixed with the nonmagnetic magnesium cations Mg^{2+} along the six nonequivalent sites of the trigonal crystal lattice that is described by the space group $P1$.

Acknowledgments

The authors would like to thank the Krasnoyarsk Regional Research Equipment Sharing Center of the Federal Research Center „Krasnoyarsk Science Center of the Siberian Branch of the Russian Academy of Sciences“ for providing the equipment needed to examine the structural properties and measure the EPR characteristics.

Funding

The study was carried out within the range of research topics under the state assignment of the Kirensky Institute of Physics, SB RAS.

Conflict of interest

The authors declare that they have no conflict of interest.

References

[1] T.V. Drokina, G.A. Petrakovskii, O.A. Bayukov, A.M. Vorotynov, D.A. Velikanov, M.S. Molokeev. Phys. Solid State **58**, *10*, 1981 (2016).

[2] T.V. Drokina, G.A. Petrakovskii, O.A. Bayukov, M.S. Molokeev, A.M. Vorotynov, S.I. Popkov, D.A. Velikanov. Phys. Solid State **62**, *2*, 297 (2020).
[3] T.V. Drokina, D.A. Velikanov, O.A. Bayukov, M.S. Molokeev, G.A. Petrakovskii. Phys. Solid State **63**, *5*, 802 (2021).
[4] T.V. Drokina, M.S. Molokeev, O.A. Bayukov, D.A. Velikanov, A.M. Vorotynov, G.A. Petrakovskii. FTT **66**, *8*, 1363 (2024). (in Russian).
[5] D.A. Velikanov. Inorg. Mater. Appl. Res. **11**, *4*, 801 (2020).
[6] F.D. Martin, H. Müller-Buschbaum. Z. Naturforschung B **50**, *1*, 51 (1995).
[7] Bruker AXS TOPAS V4: General profile and structure analysis software for powder diffraction data. User's Manual. Bruker AXS, Karlsruhe, Germany (2008).
[8] I.Ya. Korenblit, E.F. Shender. Sov. Phys. — Uspekhi **32**, *2*, 139 (1989).
[9] J.A. Mydosh. Spin-Glasses: An Experimental Introduction, Taylor and Francis, New York (1993).
[10] A.P. Ramirez. Annu. Rev. Mater. Sci. **24**, 453 (1994).
[11] J.E. Greedan. J. Mater. Chem. **11**, *1*, 37 (2001).

Translated by M.Shevelev